A Decentralized Nonlinear Harmonic Power Sharing Scheme Considering Harmonic Residual Capacity and Working Conditions of Fundamental Load

Xiao Zhang, *Student Member, IEEE*, Hao Yi, *Member, IEEE*, Ya Wen, Zhenxiong Wang, *Member, IEEE*, Qiru Li, Fangrui Kang, and Fang Zhuo, *Member, IEEE*

***Abstract*—The proper harmonic power sharing in an islanded microgrid plays a significant role in reliable system operation. Virtual-impedance-or-admittance-based strategies are intuitive and effective solutions. However, there is an inherent tradeoff between harmonic sharing accuracy and power quality. Besides, optimal capacity utilization has not been considered in most existing methods. Facing these issues, a nonlinear droop scheme, between harmonic residual capacity (HRC) and virtual impedance, is proposed in this article. Under the proposed scheme, harmonic residual capacity is defined and utilized to share harmonic power. Different working conditions of the fundamental load and corresponding control target are analyzed to determine the variable droop coefficient. Therefore, the proposed scheme can render an optimal utilization of the converter capacity and adjust the inherent tradeoff dynamically and adaptively. It contributes to a more flexible harmonic sharing in the islanded microgrid and enhances the ability to avoid overload risk. Furthermore, the communication line is unnecessary, leading to high reliability and expandability. Finally, the feasibility and effectiveness of the scheme are verified by simulation and experimental results.**

***Index Terms*—Communication-less control, harmonic power sharing, harmonic residual capacity, nonlinear droop scheme.**

Nomenclature

DG	Distributed generation.
HRC	Harmonic residual capacity.
ILR	Inner loop reconfiguration.
PCC	Point of common coupling.
PR	Proportional-resonant.
PWM	Pulse width modulation.
R-APF	Resistive active power filter.
rms	Root-mean-square.
TTA	Time-domain-based transformation algorithm.
THD	Total harmonic distortion.
VIA	Virtual impedance or admittance.
i_{h}	Harmonic current of the DG unit.
i_{L}	Filter inductor current of the DG unit.
i_{o}	Output current of the DG unit.
m	Constant coefficient in the proposed scheme.
λ_{m}	Variable coefficient in the proposed scheme.
R_{h}	Virtual impedance value under R-APF.
S_{hr}	Harmonic residual capacity of the DG unit.
S_{h}	Harmonic power.
S_{hrs12}	Threshold value between light and normal fundamental load conditions.
S_{hrs23}	Threshold value between normal and heavy fundamental load conditions.
u_{Cf}	Filter capacitor voltage of the DG unit.
Z_{line}	Line impedance of the DG unit.
Z_{ht}	Equivalent impedance of the microgrid.
Z_{omax}	Maximum VIA value in normal condition.
Z_{omin}	Minimum VIA value in the proposed scheme.
Z_{ref}	Reference value of VIA implementation.

Manuscript received 25 February 2024; revised 14 June 2024; accepted 17 July 2024. Date of publication 23 July 2024; date of current version 11 September 2024. This work was supported in part by the National Natural Science Foundation of China under Grant 51977172 and in part by the Natural Science Foundation of Shaanxi Province under Grant 2023-JC-QN-04. Recommended for publication by Associate Editor S. Golestan. *(Corresponding author: Hao Yi.)*

The authors are with the School of Electrical Engineering, Xi'an Jiaotong University, Xi'an 710049, China (e-mail: zx5201314@stu.xjtu.edu.cn; yi_hao@xjtu.edu.cn; wen_ya@stu.xjtu.edu.cn; wzhenxiong@xjtu.edu.cn; liqr0912@stu.xjtu.edu.cn; frkang@stu.xjtu.edu.cn; zffz@mail.xjtu.edu.cn).

Color versions of one or more figures in this article are available at https://doi.org/10.1109/TPEL.2024.3432187.

Digital Object Identifier 10.1109/TPEL.2024.3432187

I. Introduction

NOWADAYS, DGs, like wind turbines, photovoltaic (PV) generation, and energy storage, have attracted more attention due to their great benefits [1], [2]. They are usually connected to the PCC interfaced by a power electronic converter, ensuring the flexibility, intelligence, and reliability of DG systems, which is known as a microgrid [3], [4]. The microgrid can operate in grid-connected or islanded mode [5], [6]. In islanded mode, droop control has been proposed and is well accepted to ensure proper power sharing independent of the communication line [7]. However, traditional droop control is incapable of dealing with harmonic power-sharing issues caused by the mismatch of line impedance [8]. Harmonic current may lead to DG overload or trigger current protection if not properly shared. Hence, the rational design of the harmonic sharing strategy is significant.

Impedance-reshaping-based sharing strategies are intuitive and effective solutions to harmonic power-sharing issues [9]. Deng et al. [10] shows that one type is the ILR based strategy [11], [12], [13], [14], [15], and the other type is based on VIA [16], [17], [18], [19], [20], [21], [22], [23], [24], [25], [26],

[27], [28], [29], [30], [31], [32]. Three kinds of methods are often applied in VIA: fixed-VIA (FVIA) based strategies [16], [17], [18], [19], [20], adaptive-VIA-regulation (AVIAR) based strategies [21], [22], [23], [24], [25], [26], and VIA-droop-based strategies [27], [28], [29], [30], [31], [32].

In [11] and [12], the output current feedforward is utilized to reconfigure the inner loop structure and consequently adjust the impedance of the DG at harmonic frequencies. Similarly, harmonic current feedforward is used in [13]. By modifying the control structure, harmonic sharing accuracy can be improved, but these methods are sensitive to the system parameters. The other way is inner-loop regulator parameters adjustment, which also reshapes the DG impedance [14]. However, a communication line is needed in these strategies and system stability may be threatened. This kind of method adjusts the impedance to a certain extent, inferior to inserting an additional impedance. Therefore, VIA is more effective.

FVIA-based strategies are the simplest way to insert a virtual impedance and improve harmonic sharing. In [15], a fixed virtual resistance is introduced at harmonic frequencies and a similar idea is also applied in [16]. Furthermore, the virtual impedance can be designed separately at different frequencies [17]. However, to obtain relatively accurate harmonic sharing, the FVIA must be much larger than the line impedance, leading to voltage distortion. The conflict between harmonic sharing and power quality is irreconcilable. In [18], a virtual capacitive impedance is designed for inductive line impedance to ensure the power quality. Han et al. [19] introduced a negative virtual to improve the power quality, which causes stability issues.

Accordingly, FVIA-based methods are short of flexibility and the inherent tradeoff issue is serious. AVIAR-based strategies have shown greater performance. The primary idea of AVIAR is to insert the virtual impedance under the condition that the sum of all the virtual impedances is zero. Thus, the power quality can be effectively improved while harmonic sharing is achieved. A microgrid central controller or low-bandwidth communication is required to generate the reference signal [20], [21], [22]. To reduce the communication burden, the event trigger method [23], iterative algorithm [24], and distributed control [25] are applied. Nevertheless, communication is always required to exchange information among DGs, which is expensive and leads to degradation of reliability and expansibility.

VIA-droop-based strategies can improve harmonic sharing performance without communication lines, which are more flexible than FVIA-based methods. They are realized by establishing a droop relationship between VIA and selected control variables of DG, such as virtual resistance versus apparent power [26], virtual conductance versus harmonic current [27], and virtual inductance versus the frequency of an injected small ac signal [28]. These strategies are based on linear droop curves, indicating a fixed tradeoff between harmonic sharing and power quality. The tradeoff is roughly adjusted dynamically in [29]. A nonlinear droop scheme is a potential solution, under which the droop coefficient is not constant. Razi et al. [30] and Zhang et al. [31] showed its application but harmonic sharing is not discussed.

In most existing strategies [11], [12], [13], [14], [15], [16], [17], [18], [19], [20], [21], [22], [23], [24], [25], [26], [27], [28], [29], [30], [31], the harmonic power is shared according to the DG-rated capacity, while considering the utilization rate and flexibility is also essential in practice [10]. Mousazadeh Mousavi et al. [32] and Zeng et al. [33] considered these aspects by introducing HRC. HRC truly determines the ability of the converter to provide harmonic power. Sharing harmonic power according to HRC is an effective way to realize an optimal utilization of converter capacity and achieve flexible harmonic power sharing among DGs. However, the derivation of the working principle is not clear in [32] and [33]. Besides, the detailed parameter design method is not mentioned and the necessity of using HRC is not proved.

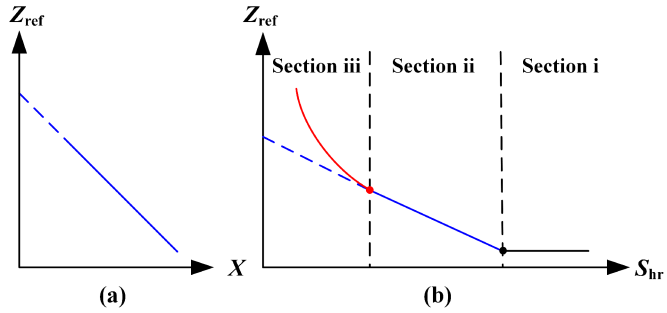

Fig. 1. Schematic diagram of the droop curve. (a) Traditional linear droop. (b) Proposed nonlinear droop.

In response to the above issues, a decentralized nonlinear droop scheme, between the HRC and VIA, is proposed in this article. The schematic diagram of the droop curve is illustrated in Fig. 1, where $Z_{\rm ref}$ is the reference VIA value, X is the selected control variable in existing methods, and $S_{\rm hr}$ is the HRC of the DG, respectively. The nonlinear droop curve is divided into three parts according to $S_{\rm hr}$, corresponding to the working conditions of low, normal, and high penetration rates of the fundamental load. A small VIA value in Section I can ensure the power quality. In Section II, the droop curve helps to share harmonic power among DGs according to the HRC. In Section III, the rapidly increasing VIA value can protect the DG with tiny HRC from overload. Therefore, the proposed scheme considers a flexible harmonic sharing and a dynamic tradeoff under various fundamental load conditions. The main contributions are summarized as follows.

1) A nonlinear droop scheme is proposed based on the mathematically formulated issue analysis. Its droop coefficient varies with the different fundamental load conditions, where the HRC of the converter changes. This helps dynamically adjust the tradeoff between power quality and harmonic sharing.
2) The necessity and advantage of using HRC are discussed. Then, harmonic power is shared according to HRC rather than the rated capacity of the converter, thus rendering an optimal utilization of converter capacity.
3) Proper parameter design of the nonlinear droop curve, including the maximum and minimum VIA value, and constant and variable droop coefficient, is provided. The proposed droop-based tuning method can be adopted to

TABLE I
COMPARISON OF EXISTING METHODS AND THE PROPOSED SCHEME

Strategy	Advantage	Disadvantage
ILR [11], [12], [13], [14]	1) Improved harmonic power sharing. 2) Good power quality.	1) Requiring deploying communication lines. 2) Sensitive to parameters.
FVIA [15], [16] [17], [18], [19]	1) Easy to implement. 2) Effectively adjusting impedance mismatch.	1) Inherent trade−off between harmonic sharing and power quality. 2) Short of flexibility.
AVIAR [20], [21], [22] [23], [24], [25]	1) Highly accurate harmonic sharing. 2) Good power quality.	1) Requiring deploying communication lines.
Linear VIA Droop [26], [27], [28], [29]	1) Independent of using communication lines. 2) Improved harmonic power sharing.	1) Fixed trade−off between harmonic sharing and power quality.
Nonlinear VIA Droop [30],[31]	1) High flexibility. 2) Dynamic trade−off.	1) Not applicable in harmonic power sharing.
Proposed Scheme	1) High flexibility and dynamic trade−off. 2) Independent of using communication line. 3) Improved harmonic power sharing. 4) Considering HRC.	\

TABLE II
SIMULATION PARAMETERS

Symbol	Description	Value
Vdc	Dc voltage	800 V
Vac	the Amplitude of ac output voltage	311 V
Z_{line1}	Line impedance of DG_1	1.2 mH
Z_{line2}	Line impedance of DG_2	0.6 mH
Z_{line3}	Line impedance of DG_3	1.2 mH
S_{rate1}	Rated capacity of DG_1	110 kVA
S_{rate2}	Rated capacity of DG_2	85 kVA
S_{rate3}	Rated capacity of DG_3	125 kVA
S_{hrs12}	theHarmonic residual capacity threshold value of section i and section ii	70 kVA
S_{hrs23}	theHarmonic residual capacity threshold value of section ii and section iii	20 kVA
Z_{omax}	the Maximum virtual impedance value of the droop curve in section ii	0.305 Ω
Z_{omin}	the Minimum virtual impedance value of the droop curve in section ii	0.10 Ω
m	Constantdroop coefficient in section ii	4.1e-6
n_{ac}	Accommodation coefficient	1.25
k_{p1}	*P-ω* droop coefficient of DG_1	6e-6
k_{p2}	*P-ω* droop coefficient of DG_2	8.6e-6
k_{p3}	*P-ω* droop coefficient of DG_3	6e-6
k_{q1}	*Q-E* droop coefficient of DG_1	1e-5
k_{q2}	*Q-E* droop coefficient of DG_2	1e-5
k_{q3}	*Q-E* droop coefficient of DG_3	1e-5
ω_0	Nominal fundamental frequency	100π rad/s
E_0	Nominal fundamental phase voltage amplitude	311 V
f_s	Switching frequency	20 kHz

improve the controllability and flexibility of designing VIA values and can be extended to other VIA methods.

The advantages and disadvantages of existing methods and the proposed scheme are compared in Table I.

The rest of this article is organized as follows. Formulated analysis of the harmonic power sharing issue, the concept of HRC, and HRC necessity are discussed in Section II. Various working conditions of DGs and nonlinear harmonic power sharing scheme design are given in Section III. Section IV presents the specific parameter design based on actual constraints and stability analysis. Moreover, simulation and experimental verification are introduced in Section V. Finally, Section VI concludes this article.

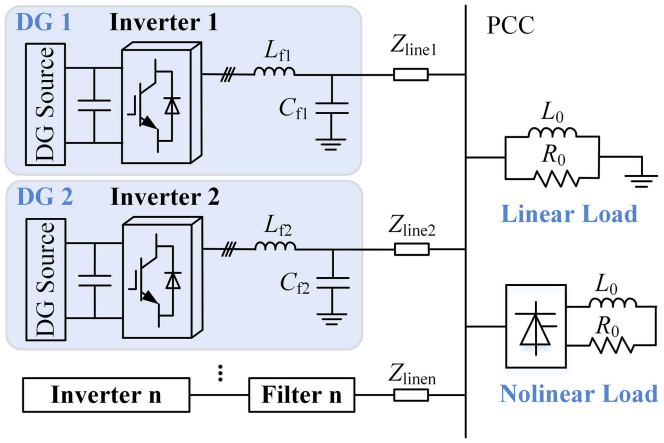

Fig. 2. Topology of islanded microgrid integrated with n-DG.

II. HARMONIC SHARING ISSUE AND HARMONIC RESIDUAL CAPACITY ANALYSIS

In this part, the harmonic sharing issue is analyzed, based on the basic control structure of the microgrid and equivalent harmonic circuit model. Furthermore, the definition of HRC and its necessity are discussed.

The topology of a sample islanded microgrid integrated with n-DGs is illustrated in Fig. 2, where subscript n indicates the *n*th DG, Z_{line} is the line impedance, and L_f and C_f are filter inductor and capacitor, respectively. All DG sources are connected to the PCC interfaced by inverters, feeding linear, and nonlinear loads. For the sake of clarity, n is ignored in the following derivation.

A. Basic Control Structure Applying Droop Control

In islanded mode, each DG is controlled as a voltage source to maintain the voltage and frequency support for loads. To achieve the fundamental active and reactive power sharing among DGs, droop control is generally used, shown as

$$\begin{cases} \omega_{ref} = \omega_0 - k_P (P - P_{ref}) \\ E_{ref} = E_0 - k_Q (Q - Q_{ref}) \end{cases} \tag{1}$$

where ω_{ref} and E_{ref} are angular frequency and amplitude of voltage reference value, ω_0 and E_0 are those of rated value, k_P and k_Q are active and reactive droop coefficient, P and Q are actual active and reactive power of inverter, and P_{ref} and Q_{ref} are reference value of active and reactive power, respectively.

It should be noticed that (1) is derived in a microgrid with mainly inductive line impedance, while the feeder impedance is mainly resistive in a low-voltage microgrid [8]. In this case, the droop control is alternatively considered as (2).

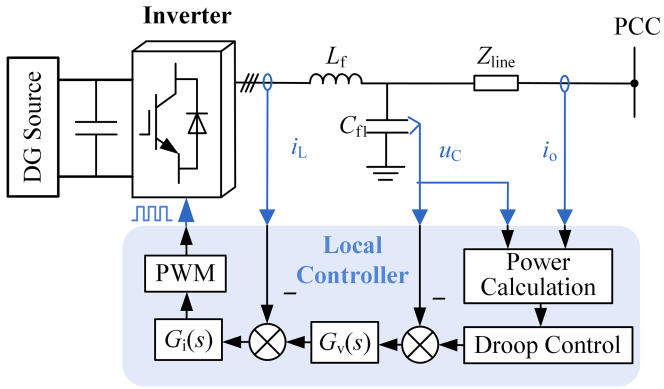

Fig. 3. Basic control structure of the inverter.

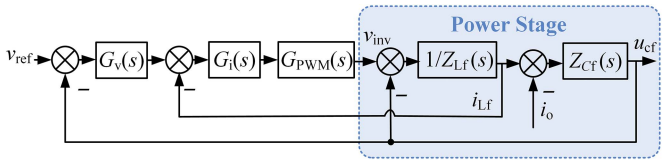

Fig. 4. Equivalent control model of the inverter.

Accordingly, the basic control structure is drawn in Fig. 3, where i_{Lf} is the filter inductor current, i_{o} is the output current, u_{Cf} is the filter capacitor voltage, $G_{\mathrm{v}}(s)$ is the outer voltage controller, and $G_{\mathrm{i}}(s)$ is the inner current controller, respectively, as follows:

$$\begin{cases} \omega_{ref} = \omega_0 + k_Q \left(Q - Q_{ref}\right) \\ E_{ref} = E_0 - k_P \left(P - P_{ref}\right). \end{cases} \tag{2}$$

Fig. 4 shows the equivalent control block diagram of the inverter, where $G_{\mathrm{PWM}}(s)$ is the transfer function of PWM, $Z_{\mathrm{Lf}}(s)$ is that of $\mathrm{L_f}$, $Z_{\mathrm{Cf}}(s)$ is that of $\mathrm{C_f}$, v_{ref} is the voltage reference value obtained by droop control, and v_{inv} is the output voltage of the inverter, respectively. Accordingly, the power stage can be expressed as

$$\begin{aligned} i_{L_f}(s) = & \underbrace{\frac{1}{Z_{Lf}(s) + Z_{Cf}(s)}}_{Y(s)} v_{inv}(s) \\ & + \underbrace{\frac{Z_{Cf}(s)}{Z_{L_f}(s) + Z_{Cf}(s)}}_{Z(s)} i_o(s). \end{aligned} \tag{3}$$

According to (3), Fig. 4 can be simplified to Fig. 5. Therefore, utilizing the superposition theorem and Mason's gain formula, the inverter controlled as a voltage source can be expressed as

$$u_{Cf}(s) = G_{\mathrm{CV}}(s) v_{ref}(s) - Z_{ov}(s) i_o(s). \tag{4}$$

The detailed expression of $G_{\mathrm{CV}}(s)$ and $Z_{\mathrm{ov}}(s)$ is given in the Appendix. Equation (4) indicates that the DG is equivalent to a voltage source controlled by $G_{\mathrm{CV}}(s)$ and $v_{\mathrm{ref}}(s)$, in series with the output impedance $Z_{\mathrm{ov}}(s)$.

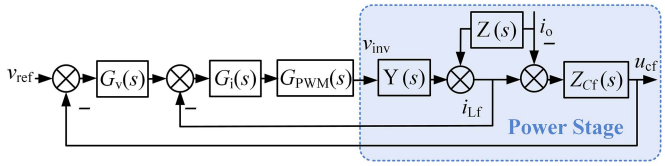

Fig. 5. Simplified equivalent control model of the inverter.

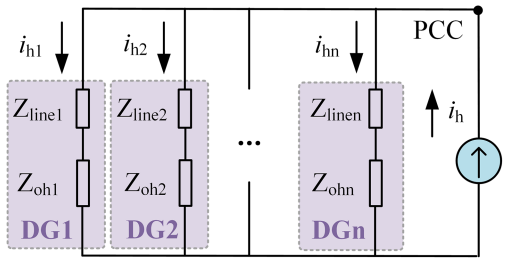

Fig. 6. Equivalent harmonic circuit of an n-DG microgrid.

B. Harmonic Sharing Issue Analysis

According to (4), under the basic control, v_{ref} is obtained by droop control, in which only fundamental components are considered. Therefore, the equivalent harmonic circuit with n-DGs can be obtained in Fig. 6, where Z_{oh} is the harmonic component of $Z_{\mathrm{ov}}(s)$, indicating the equivalent harmonic impedance. The nonlinear load is represented by a current source i_{h}. Based on Fig. 6, the harmonic sharing issue is mathematically formulated and analyzed as follows.

The harmonic current flowing into nth DG is calculated as

$$i_{hn,k} = \frac{Z_{ht,k}}{Z_{linen,k} + Z_{ohn,k}} i_{h,k} \tag{5}$$

where subscript k represents the harmonic component of kth order, and Z_{ht} is the equivalent impedance of the whole network, obtained by

$$\frac{1}{Z_{ht,k}} = \sum_{i=1}^{n} \frac{1}{Z_{linei,k} + Z_{ohi,k}}. \tag{6}$$

Therefore, harmonic sharing is determined by the DG output harmonic impedance and line impedance. The mismatch of line impedance leads to harmonic sharing issues because Z_{oh} is always zero under the basic control scheme. That is where harmonic sharing issues come from and reshaping the output harmonic impedance of DG is an effective solution. For ease of analysis, k is omitted in the following discussion since the impedance at each harmonic order is the same in this article.

According to IEEE standard 1459-2010 [34], the harmonic power is defined

$$\begin{aligned} S_h &= \sqrt{D_c^2 + D_v^2 + D_h^2} = 3\sqrt{V_f I_h + V_h I_f + V_h I_h} \\ &\approx 3 V_f I_h = 3 V_f \sqrt{\sum\nolimits_k I_{h,k}^2} \end{aligned} \tag{7}$$

where S_{h} is harmonic power, D_{c} is current distortion power, D_{v} is voltage distortion power, D_{h} is harmonic apparent power, V

is the root-mean-square (rms) value of DG output voltage, I is the rms value of DG output current, and subscript f and h are fundamental and harmonic component, respectively. In a regular microgrid, PCC voltage quality must be ensured, which means the harmonic voltage can be ignored and the approximate result is obtained.

Correspondingly, the harmonic power sharing error between ith and jth DG is expressed in

$$S_{h,i,j} = |\alpha_i S_{hi} - \alpha_j S_{hj}| \quad (1 \le i \le j \le n) \tag{8}$$

where α_n is the harmonic sharing coefficient of nth DG, which indicates the harmonic sharing principle. Therefore, the proportional relationship between α_i is α_j is meaningful. Set α_1 at 1, and others can be obtained.

Normally, without a harmonic sharing strategy, each α is the same. In this case, the harmonic power is shared according to the line impedance. $S_{h,i,j}$ increases with the increase of line impedance mismatch, reflecting the harmonic sharing issues in an islanded microgrid.

While utilizing VIA, the equivalent harmonic impedance of the inverter is reshaped and the harmonic sharing is modified to minimize the $S_{h,i,j}$. If each α is still the same, the harmonic power will be equally shared among DGs when the $S_{h,i,j}$ is minimized to zero. The sharing principle is unreasonable because harmonic power is expected to be shared according to DG's rated capacity. Thus, in most existing methods [15], [16], [17], [18], [19], [20], [21], [22], [23], [24], [25], [26], [27], [28], [29], the α_n is designed following (9), where S_{raten} is the rated capacity of the nth DG

$$\alpha_1 S_{\text{rate1}} = \alpha_2 S_{\text{rate2}} = \cdots = \alpha_n S_{raten}. \tag{9}$$

Accordingly, when the $S_{h,i,j}$ is minimized to zero, the harmonic power is properly shared referring to the S_{raten}, which is reasonable and can avoid DG overload in most cases.

C. Harmonic Residual Capacity Analysis

Traditional methods following (9) can handle most of the working conditions and enhance harmonics sharing to avoid DG overloaded, to a certain degree. However, the ability of nth DG to absorb harmonic power is determined by its HRC. HRC is defined as

$$S_{hrn} = \sqrt{S_{raten}^2 - S_{fn}^2} = \sqrt{S_{raten}^2 - P_n^2 - Q_n^2} \tag{10}$$

where S_{fn} is the fundamental power of nth DG.

Therefore, the existing methods, which share harmonic power according to the rated capacity of DG, show the following shortcomings.

1) The active power of PVs and wind turbines highly depends on the natural environment (i.e., wind speed and illumination intensity). Besides, the output power of the energy storage devices is related to their state of charge [35]. Therefore, even with the same power rating, the output active power of DGs may vary and their HRCs are different. In this case, the upper limit of harmonic power absorbed by the microgrid will be restrained by the DG with the smallest HRC. The conventional strategies are weak to deal with the conditions with a high penetration rate of nonlinear load. DG overload may occur even if the whole microgrid can provide more harmonic power, indicating a poor capacity utilization rate.
2) The tradeoff between harmonic sharing and power quality is fixed under existing methods. However, in various working conditions, the control priority of the system is different. It is preferred to dynamically adjust the tradeoff according to actual situations, which can greatly improve the flexibility of the microgrid and achieve a high-quality operation.

HRC is an effective solution to these issues. On the one hand, sharing harmonic power among DGs according to their HRCs can render an optimal utilization of DG capacity. The ability of the microgrid to feed nonlinear load can be enhanced. On the other hand, different working conditions can be reflected in HRC. Thus, the tradeoff can be dynamically adjusted according to the states of HRC. To sum up, utilizing HRC in a harmonic sharing strategy is of great necessity and significance. Detailed strategy design will be provided in Section III.

III. Nonlinear Harmonic Sharing Scheme Design

According to the analysis in Section II, achieving harmonic power sharing by HRC is an effective way to improve the microgrid performance faced with high penetration of nonlinear loads. Based on this idea, a nonlinear harmonic sharing scheme considering HRC and working conditions of fundamental load is proposed.

A. Overall Control Structure Using Proposed Scheme

Fig. 7 illustrates the overall control strategy using the proposed nonlinear harmonic sharing scheme, where subscript f and h represent fundamental and harmonic components, subscript α and β are the components in α and β coordinate system after Clark transformation, Z_{ref} is the reference virtual impedance value for VIA implementation, Z_{v} is the virtual impedance, v_{ref} represents reference value of outer voltage loop obtained by fundamental droop control, and i_{ref} is the reference value of inner current loop, respectively.

The fundamental control scheme has been introduced in Section II, according to which the fundamental component of i_{ref} is generated. The core technology of the proposed harmonic sharing scheme is a nonlinear droop curve between Z_{ref} and S_{hr} using a variable droop coefficient, with the help of which a dynamically regulated VIA reference value is obtained. That is the main innovation of this article and it will be detailly analyzed in Section II-B. Fig. 7 also demonstrates two other significant elements of the control strategy, which are the harmonic extraction method and VIA implementation. They will be introduced in Sections II-C and II-D.

As modeled in Section II, by reshaping the equivalent impedance of DGs, the harmonic power sharing among DGs can be adjusted adaptively, according to the HRC and different working conditions of fundamental load. The whole impedance

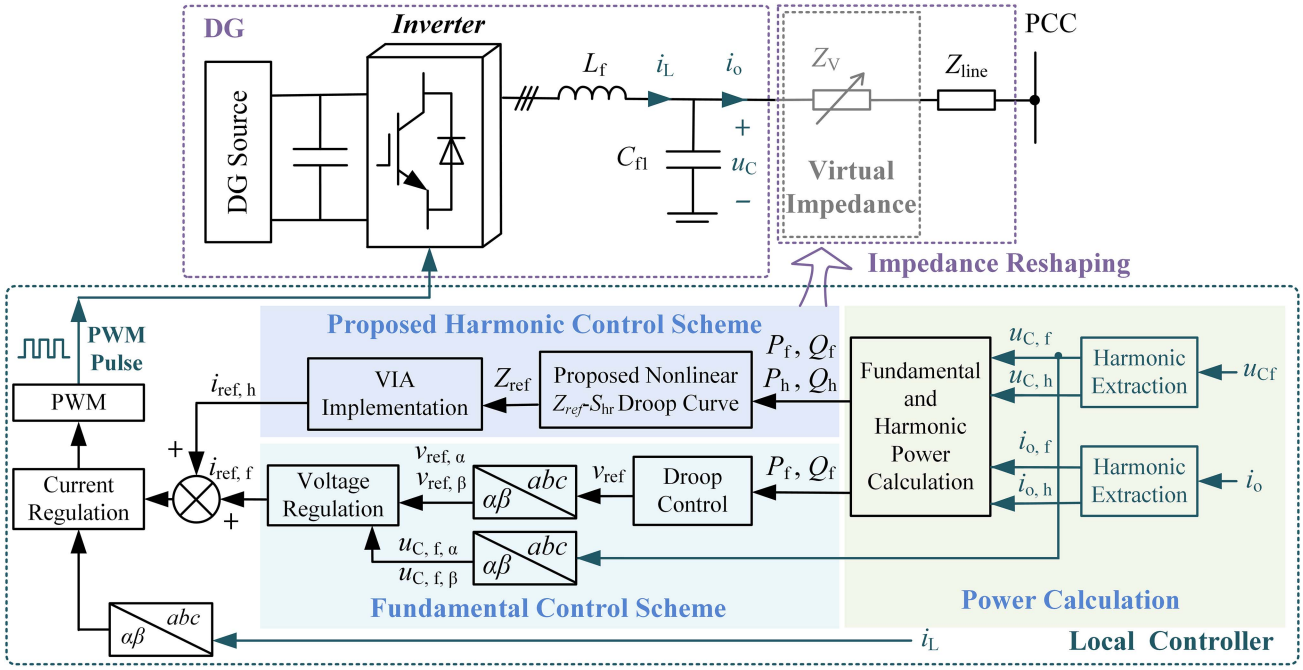

Fig. 7. Overall control strategy using the proposed nonlinear harmonic sharing scheme.

of DG after implementing VIA is rewritten as

$$Z_{\mathrm{DG}n,h} = Z_{linen,k} + Z_{ohn,k} = Z_{refn} \tag{11}$$

where $Z_{\mathrm{DG}n,h}$ is the overall equivalent harmonic impedance of nth DG. The virtual impedance at kth order harmonic is set at the same value, thus, subscript k is ignored in the following derivation for ease of analysis.

B. Design of Nonlinear Droop Curve

Before designing the Z_{ref} - S_{hr} droop curve, different working conditions of DGs should be analyzed, thereby prioritizing control objectives. For ease of analysis, a microgrid composed of two DGs is considered to conclude different working conditions and corresponding control targets. Distinguished by the penetration rate of fundamental load and HRC, the following working conditions can be defined.

Condition of light fundamental load: under a low level of fundamental loads, the HRC of DG_1 and DG_2 are quite enough, facing no DG overload risk. Therefore, power quality enhancement is before the harmonic sharing accuracy. In this case, the virtual impedance can be set at a relatively small value to reduce the THD of PCC voltage. Indeed, it is even acceptable not to deal with harmonic sharing, due to adequate S_{hr1} and S_{hr2}.

Condition of normal fundamental load: with the increasing penetration rate of fundamental loads, S_{hr} reduces to a normal range. This condition is commonly taken into consideration under most of the existing methods and an inherent tradeoff is designed properly. The harmonic power should be shared according to the HRC of DGs and a constant-coefficient droop relationship between S_{hr} and Z_{ref} is established. The derivation process of the droop curve is as follows.

Substituting from (11) to (8), the harmonic current sharing error is expressed as

$$\triangle\, i_h = i_{h1} - i_{h2} = Z_{ht} i_h \left(\frac{1}{Z_{ref1}} - \frac{1}{Z_{ref2}} \right). \tag{12}$$

According to (6)

$$Z_{ht} = \frac{Z_{ref1} Z_{ref2}}{Z_{ref1} + Z_{ref2}}. \tag{13}$$

Thus, (12) is simplified as

$$\Delta i_h = \frac{i_h}{Z_{ref1} + Z_{ref2}} \left(Z_{ref2} - Z_{ref1} \right). \tag{14}$$

The harmonic sharing error is determined by the matching degree of Z_{ref}, indicated by Z_{ref2} minus Z_{ref1}. To share harmonic power by S_{hr}, a negative correlation between them should be ensured, shown as

$$\frac{Z_{ref2} - Z_{ref1}}{S_{hr2} - S_{hr1}} = -m \tag{15}$$

where m is the correlation coefficient. Therefore, the droop curve can be obtained based on (15), expressed as

$$Z_{ref} = Z_0 - m S_{hr} \tag{16}$$

where Z_0 is the designed value of Z_{ref} when S_{hr} is zero.

Design Z_{ref} according to (16), and the harmonic power sharing will be shared by S_{hr} automatically, without using communication. When S_{hr1} is the same as S_{hr2}, the harmonic power is shared equally, which is the application of the conventional sharing strategy based on rated capacity. This means the proposed scheme in this article can also cover the function of traditional methods. Noting that greater Z_{ref} leads to more

accurate harmonic sharing, as shown in (14), but results in worse power quality, this is an embodiment of inherent tradeoff. Hence, the range of Z_{ref} must be designed carefully and it will be discussed in Section IV.

Condition of heavy fundamental load: under a higher penetration of fundamental loads, the S_{hr} of one DG is normal, while that of the other one is at a low value, facing the risk of overload. In this case, the latter one must automatically adjust its VIA and force the harmonic power into the former one. In this way, the microgrid can continue to maintain stable and safe operation, thus rendering an optimal utilization of DG capacity. The conventional fixed harmonic droop control cannot deal with this issue [26], [27], [28], [29]. In this case, the primary task of the control strategy is to ensure the safe operation of the system without overload, and the power quality can deteriorate slightly to ensure harmonic distribution. This represents the dynamic tradeoff adjustment. The Z_{ref} of DG with low S_{hr} is designed following the principle below:

$$Z_{ref} = Z_{va} - \lambda_m m S_{hr} \ (\lambda_m > 1) \tag{17}$$

where λ_m is the variable coefficient and Z_{va} is the bias that varies with working conditions. In this case, Z_{ref} is supposed to rise rapidly so that the harmonic current flowing into the DG can be reduced quickly. This requires a sharper droop curve than the condition of normal fundamental load, indicating a larger absolute value of the droop coefficient. Thus, the λ_m is larger than 1. Under the action of Z_{va} and λ_m, the DG with low S_{hr} will rapidly raise its harmonic impedance and force the harmonic current into other DGs. The value of λ_m is determined by the actual demands. There is no theoretical maximum restraint of λ_m because the primary objective is protecting the DG from overload. Their design principle is discussed in Section IV.

Condition of overloaded fundamental load: under a very high level of fundamental loads, both the S_{hr} of DG_1 and DG_2 are insufficient. The DGs are faced with a great risk of overload, and they cannot force the harmonic current into others because other DGs are not able to consume more harmonic power. This indicates the upper limit of the microgrid absorbing harmonic power. In this case, superior-level scheduling intervention is required for load reduction or capacity expansion. This extreme case is beyond the scope of this article, and the proposed scheme can help to generate an alerting signal by aggravating PCC power quality substantially.

To sum up, the light-fundamental-load and normal-fundamental-load conditions are regular working conditions, while heavy-fundamental-load and overloaded-fundamental-load conditions are emergency conditions facing overload risk. Accordingly, the Z_{ref} - S_{hr} nonlinear droop curve in various fundamental load conditions can be drawn in Fig. 8. When both two DGs are in Section I, it represents the condition of the light fundamental load. While they are in Section II, it is the condition of the normal fundamental load. The condition of the heavy fundamental load is special, where one DG is in Section III and the other one is in Section II. Fig. 8 shows the core technology of the proposed nonlinear harmonic sharing scheme and it can

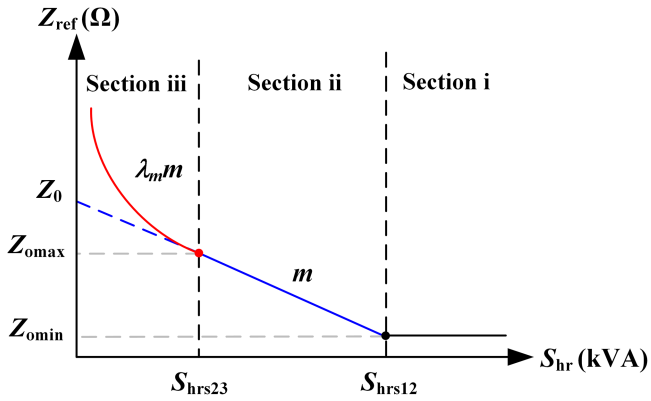

Fig. 8. Proposed Z_{ref} – S_{hr} nonlinear droop curve.

be expressed as

$$Z_{ref} = \begin{cases} Z_{o\min} & (S_{hr} \geq S_{hrs12}) \\ Z_0 - mS_{hr} & (S_{hrs23} \leq S_{hr} \leq S_{hrs12}) \\ Z_{va} - \lambda_m m S_{hr} & (S_{hr} \leq S_{hrs23}) \end{cases} \tag{18}$$

where S_{hrs12} is the threshold value to distinguish the condition of light and normal fundamental load, and S_{hrs23} is that to distinguish the condition of normal and heavy fundamental load. As a result, using (18), α_n in (9) is designed as (19). The specific parameter design of (18) will be provided in Section IV

$$\alpha_1 S_{hr1} = \alpha_2 S_{hr2} = \cdots = \alpha_n S_{hrn}. \tag{19}$$

It should be noted that the conclusion can be extended to a microgrid integrated with n-DGs. Once considering the n-DG microgrid, the combination of DG's S_{hr} conditions will greatly increase. Therefore, based on different primary objectives of the control strategy, the generalized working conditions under an n-DG microgrid are defined as follows.

1) The condition of light fundamental load: S_{hr} of all DGs is in Section I of Fig. 8.
2) The condition of normal fundamental load: the S_{hr} of at least one DG is in Section II, while the others are in Sections II or I. The Z_{ref} of DGs in Section II satisfies (20) and the harmonic power is shared according to the HRC of DGs

$$\frac{Z_{refi} - Z_{refj}}{S_{hri} - S_{hrj}} = -m \ (1 \leq i < j \leq n). \tag{20}$$

3) The condition of heavy fundamental load: the S_{hr} of one DG is in Section III, while others are in Sections II or I.
4) The condition of overloaded fundamental load: more than one DG faces overload risk and the S_{hr} of them is in Section III.

The harmonic sharing principle and the control target of different working conditions are the same as those analyzed based on the two-DG microgrid.

C. Harmonic Extraction Method

As shown in Fig. 7, the harmonic extraction method plays a significant role in the scheme. It is required to selectively extract significant harmonic voltage or current to improve control performance. The TTA is used in this article. It enjoys the advantage of easy implementation, rapid calculation, and signal interference immunization. Its operation principle is based on the orthogonality of trigonometric function as follows:

$$\begin{cases} \int_0^T \sin(m_0\omega t)\cos(n_0\omega t)dt = 0\,(m_0 \neq n_0) \\ \int_0^T \sin(n_0\omega t)\sin(m_0\omega t)dt = 0\,(m_0 \neq n_0) \\ \frac{2}{T}\int_0^T \sin(n_0\omega t)\sin(n_0\omega t)dt = 1 \end{cases} \tag{21}$$

where T is the period of trigonometric function.

Taking harmonic extraction of current as an example, the i_o in phase A can be expressed as

$$\begin{aligned} i_{oA} = {} & a_f \sin(\omega t + \varphi_0) + \cdots + a_k \sin(k\omega t) \\ & + b_k \cos(k\omega t) + \ldots \end{aligned} \tag{22}$$

where a_f is the amplitude of the fundamental component, φ_0 is the initial phase and ω is the fundamental angular frequency respectively. The kth-order harmonic component is represented by the sine component plus cosine component, of which the amplitude is a_k and b_k. Thus, by solving a_k and b_k, the kth-order harmonic component can be selectively extracted.

Multiply (22) by orthogonal kth-order sine and cosine function, and a_k and b_k can be solved as

$$\frac{2}{T}\int_0^T i_{oA}\sin(k\omega t)dt = ak \tag{23}$$

$$\frac{2}{T}\int_0^T i_{oA}\cos(k\omega t)dt = bk. \tag{24}$$

Therefore, a selective harmonic extraction is achieved.

D. Virtual Impedance Implementation

As mentioned before, the main contribution of the paper is proposing the nonlinear harmonic sharing scheme by generating the reference value of VIA, indicated by Z_{ref}. Thus, designing a new VIA method is beyond the scope of this article, and the existing R-APF method is selected to verify the effectiveness of the proposed scheme. It should be noted that the nonlinear harmonic sharing scheme can be applied and extended to other kinds of VIA methods.

The control structure of R-APF at selective harmonics is shown in Fig. 9, where v_{PCC} is the PCC voltage, R_{h} is the reference resistance value, and subscript h represents the harmonic component, respectively. Combining the control structure in Fig. 9 with the control model in Fig. 5, the reshaped equivalent harmonic impedance of DG is derived as

$$\begin{aligned} Z_{\mathrm{DG},h}(s) &= -\frac{v_{\mathrm{PCC},h}(s)}{i_{o,h}(s)} \\ &= \frac{R_h Z_{\mathrm{line}}(s) + R_h Z_{Cf}(s)\left[1 + G_o(s) - Z(s)\right]}{G_o(s)\,Z_{Cf}(s) + R_h} \end{aligned} \tag{25}$$

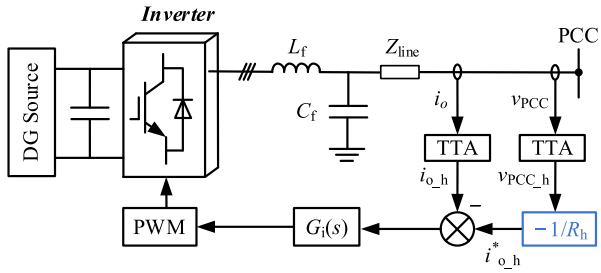

Fig. 9. Control structure of R-APF at selective harmonics.

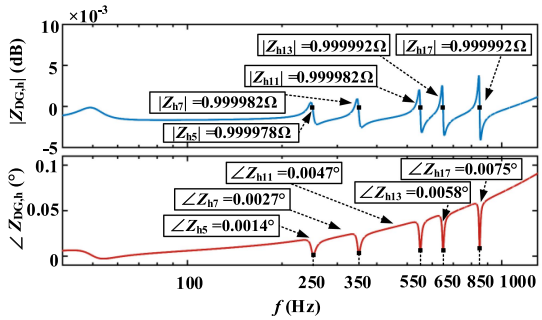

Fig. 10. Bode diagram of R-APF method.

where Z(s) is defined in (3) and G_{o}(s) is shown in Appendix. The PR controller is utilized in the current regulator to achieve a considerable gain at harmonics, thus, G_{i}(s) is expressed as

$$\begin{aligned} G_i(s) = {} & k_{pi} + \frac{2k_{rf}\omega_c s}{s^2 + 2\omega_c s + \omega_f^2} \\ & + \sum_{k=-5,7,-11,13,-17} \frac{2k_{rh}\omega_c s}{s^2 + 2\omega_c s + (k\omega_f)^2} \end{aligned} \tag{26}$$

where k_{pi} is the proportional coefficient, k_{rf} is the resonant gain at the fundamental frequency, k_{rh} is at the harmonic frequency, ω_f is the fundamental angular frequency, ω_c represents the cut-off frequency, and k denotes the harmonic order. In practice, the fundamental frequency varies with droop control, as shown in (2) and (3). Therefore, ω_f is designed by ω_{ref} adaptively to enhance control performance.

In an islanded microgrid, the diode rectifiers are the main nonlinear loads that generate harmonic power demands, where odd-order and low-order harmonic components dominate. The fifth-order, eleventh-order, and seventeenth-order harmonics are the negative-sequence components, represented by the negative signs in k. Besides, the diode rectifier generates no third harmonic. Accordingly, in (26), k is designed as −5, 7, −11, 13, and −17 [13].

The gain of the PR controller is considerably large at selected harmonics. Thus, G_{o}(s) is large enough, and (25) is simplified as

$$Z_{\mathrm{DG},h}(s) = -\frac{v_{PCC,h}(s)}{i_{o,h}(s)} \approx R_h. \tag{27}$$

The bode diagram of (25) is illustrated in Fig. 10, which indicates the virtual impedance only comes into effect at selected

harmonics and is free from the impact of the inverter closed-loop gain. The output impedance of the inverter is reshaped as R_h and the influence of line impedance is also immune.

To sum up, the nonlinear droop curve in Section III-C guides the equivalent impedance value. At the same time, the VIA method is responsible for reshaping the DG impedance to the value generated by the former. Design R_h to be the same as Z_{ref} according to (18), and the proposed nonlinear harmonic sharing scheme can be realized.

IV. Parameter Design Considering Constraints

In the proposed scheme, as shown in Fig. 8, three parameters must be carefully designed, i.e., minimum virtual impedance value Z_{omin}, maximum virtual impedance Z_{omax} in the condition of normal fundamental load, and the droop coefficient (including the constant-coefficient m and variable coefficient λ_m). In this part, the specific parameter design method considering actual constraints is introduced.

A. Design of Minimum Virtual Impedance Value

As analyzed before, the lower equivalent impedance value results in higher power quality of PCC voltage, while higher impedance value leads to more accurate harmonic sharing. In the condition of light fundamental load, the priority of the proposed scheme is power quality improvement, thus, Z_{omin} should be designed as low as possible. However, the minimum value of Z_{ref} is restrained by the system stability. According to (25), the root locus of $Z_{\text{DG},h}(s)$ with various R_h can be drawn as Fig. 11(a). With the decrease of R_h, the closed-loop pole of the control system is moved closer to the imaginary axis. Once R_h is smaller than zero, the closed-loop pole of the system is at the right half plane, indicating system instability. Therefore, the minimum virtual impedance value is supposed to be set at a positive value. Considering the influence of practical factors, e.g., error of controller and noise interference, the design margin is required. Accordingly, Z_{omin} is set at 0.1 Ω in the simulation and 0.15 Ω in the experiment.

To further prove the correctness of the above design, the Nyquist plots when R_h is equal to 0.1 Ω and minus 0.1 Ω are provided in Fig. 11(b) and (c), respectively. In Fig. 11(b), point $(-1, \text{j}0)$ is not surrounded by the Nyquist curve, indicating a stable system. Therefore, the selected minimum virtual impedance value is acceptable. While the point $(-1, \text{j}0)$ is surrounded by the Nyquist curve, as shown in Section IV-(c), this means the system is unstable when R_h is set as a negative value.

B. Design of Maximum Virtual Impedance Value

While implementing the proposed scheme, the rms value of harmonic current flowing into DG_1 is restrained by its HRC. Equation (28) can be obtained according to (5), (6), (7), and (11)

$$I_{h1} = \frac{R_{h2-n}}{R_{h1} + R_{h2-n}} I_h < \frac{S_{hr1}}{3V_{PCC,f}} \tag{28}$$

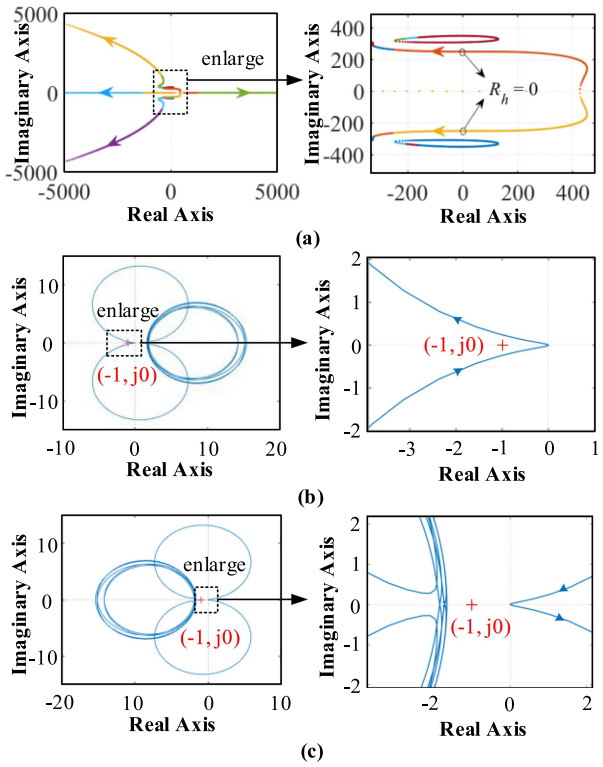

Fig. 11. Stability analysis. (a) Root locus of $Z_{\text{DG, h}}(s)$ under various R_h. (b) Nyquist plot when $R_h = 0.1\ \Omega$. (c) Nyquist plot when $R_h = -0.1\ \Omega$.

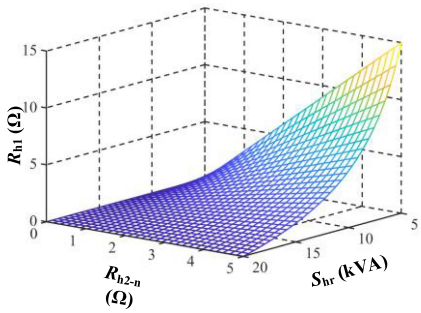

Fig. 12. Relationship among R_{h1}, S_{hr}, and $R_{h2\text{-}n}$.

where $R_{h2\text{-}n}$ represents the sum of the virtual impedance value of DG_2 to DG_n, which is shown in

$$R_{h2-n} = \sum_{i=2}^{n} R_{hi}. \tag{29}$$

By solving (28), R_{h1} is expressed as

$$R_{h1} > R_{h2-n}\left(3\frac{V_{\text{PCC},f}}{S_{hr1}} I_h - 1\right). \tag{30}$$

According to (30), the influence of $R_{h2\text{-}n}$ and S_{hr1} on R_{h1} is illustrated in Fig. 12, which means the design of R_{h1} is also affected by the virtual impedance of other DGs. The parameter design must consider a global impact. Therefore, Z_{ht}, which clusters the virtual impedance value of all DGs is considered.

Its expression is shown as (6). The increase of Z_{omax} leads to an increase in Z_{ht}. The THD of PCC voltage is calculated as

$$\mathrm{THD}_V = \frac{1}{V_{\mathrm{PCC}f}}\sqrt{\sum\nolimits_k Z_{ht,k}^2 I_{h,k}^2} \tag{31}$$

where $I_{h,k}$ is the rms value of kth order harmonic current generated by the nonlinear load. According to (6), the increase of Z_{omax} leads to an increase of $\mathrm{THD_v}$, thus, the design of maximum virtual impedance value is restrained by THD limitation and it should be designed considering the number of DGs and the THD toleration of PCC.

C. Design of Constant and Variable Droop Coefficient

After confirming Z_{omax} and Z_{omin}, the constant droop coefficient m in Section II can be obtained by (32). Accordingly, once S_{hrs12} and S_{hrs23} are determined, m can be also calculated. As mentioned before, S_{hrs12} and S_{hrs23} are used to distinguish different working conditions, thus, the definition of the light, the normal, and heavy-fundamental-load condition affects the value of S_{hrs12} and S_{hrs23}. Considering the practical situation, they are defined as (33), where min $[S_{raten}]$ is the minimum rated capacity of all the DGs in the microgrid. Combining (32) and (33), the droop coefficient m is obtained

$$m = \frac{S_{hrs12} - S_{hrs23}}{Z_{o\max} - Z_{o\min}} \tag{32}$$

$$\begin{cases} S_{hrs12} = 0.8 \sim 0.9 \min\left[S_{raten}\right] \\ S_{hrs23} = 0.2 \sim 0.4 \min\left[S_{raten}\right] \end{cases}. \tag{33}$$

Furthermore, Z_0 can be solved as

$$Z_0 = Z_{o\max} + mS_{hrs23}. \tag{34}$$

In the condition of heavy fundamental load, the DG in Section III should rapidly raise its harmonic impedance and force the harmonic current into the DG in Section II. For the sake of analysis, assume that DG_1 is in Section III and DG_2 is in Section II. The harmonic current flowing into DG_1 before and after adjusting the coefficient is expressed as (28) and (35), respectively, as follows:

$$I_{h1\_2} = \frac{R_{h2-n}}{R_{h1\_2} + R_{h2-n}} I_h \tag{35}$$

where R_{h1_2} is the VIA value using variable droop coefficient and I_{h1_2} is harmonic current flowing into DG_1. The primary control target is forcing the harmonic current less than I_{h1} divided by a constant value n_{ac}, which is expressed as (36). The n_{ac} is defined to show the control target of the proposed nonlinear droop scheme under this condition. It indicates the proportion of harmonic current reduction

$$I_{h1\_2} < I_{h1}/n_{\mathrm{ac}}. \tag{36}$$

According to (18), (28), (35), and (36), $R_{\mathrm{h1\_2}}$ can be solved as

$$\begin{aligned} R_{h1\_2} &> n_{\mathrm{ac}} R_{h1} + (n_{\mathrm{ac}} - 1) R_{h2-n} \\ &= n_{\mathrm{ac}} (Z_0 - mS_{r1}) + (n_{\mathrm{ac}} - 1) R_{h2-n}. \end{aligned} \tag{37}$$

TABLE III
WORKING CONDITION VARIATION IN SIMULATION

Time Range	Working Condition	Calculated value of $\mathrm{R_h}$
0.2–0.6 s	Light fundamental load	R_{h1}=R_{h2}=R_{h3}=0.1 Ω
0.6–1 s	Normal fundamental load	R_{h1}=0.160 Ω R_{h2}=0.129 Ω R_{h3}=0.1 Ω
1–1.4 s	Normal fundamental load	R_{h1}=0.293 Ω R_{h2}=0.161 Ω R_{h3}=0.126 Ω
1.4–1.8 s	Heavy fundamental load	R_{h1}=0.571 Ω R_{h2}=0.166 Ω R_{h3}=0.138 Ω

Design $R_{\mathrm{h1\_2}}$ following (37), and (36) can be satisfied because R_{h2} is always less than Z_{omax}

$$\begin{aligned} R_{h1\_2} &= n_{\mathrm{ac}} (Z_0 - mS_{r1}) + (n_{\mathrm{ac}} - 1)(n-1) Z_{o\max} \\ &> n_{\mathrm{ac}} (Z_0 - mS_{r1}) + (n_{\mathrm{ac}} - 1) R_{h2-n}. \end{aligned} \tag{38}$$

Therefore, the variable coefficient λ_m is calculated by

$$\lambda_m = \frac{(n_{\mathrm{ac}} - 1)\left[Z_0 + (n-1) Z_{o\max}\right] + m\left(S_{hrs23} - n_{\mathrm{ac}} S_{hr1}\right)}{m\left(S_{hrs23} - S_{hr1}\right)}. \tag{39}$$

Furthermore, Z_{va} is calculated as

$$Z_{va} = Z_0 + (\lambda_m - 1) mS_{hrs23}. \tag{40}$$

The actual residual capacity of the nth DG is defined as

$$S_{arn} = \sqrt{S_{raten}^2 - S_{fn}^2 - S_{hn}^2}. \tag{41}$$

To protect DG_1 from overload, n_{ac} should be selected carefully according to S_{ar1} and kept within a safe range by reducing the harmonic current flowing into DG_1. Because S_{ar} varies with different values of S_{hr}, the n_{ac} and corresponding λ_{m} are also changing. That is why it is called a variable droop coefficient and the droop curve in Section III is roughly equivalent to a curve with an increasing slope, as shown in Fig. 8.

V. SIMULATION AND EXPERIMENTAL VERIFICATION

To verify the effectiveness of the proposed strategy, both simulation and experimental results are conducted in this section, based on the same topology in Fig. 2.

A. Simulation Results

The continuous working conditions are simulated in MATLAB/Simulink, and the corresponding parameters are listed in Table II. The simulation model is based on the islanded microgrid integrated with three DGs. The condition variation and the relevant reference value of virtual impedance are shown in Table III.

By adding fundamental load and diode rectifier at 0.6 s, 1 s, and 1.4 s, four working conditions are simulated. As the HRC changes, their reference value of virtual impedance is calculated according to Fig. 8 and (18).

1) Nonlinear Harmonic Sharing Verification: In this article, a nonlinear harmonic sharing method, using a Z_{ref} - S_{hr} droop curve with a variable droop coefficient, is proposed. Under

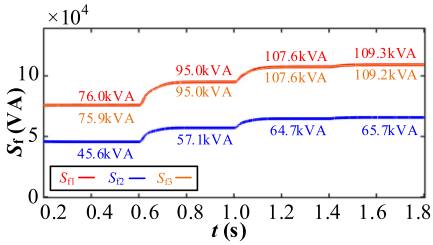

Fig. 13. Fundamental apparent power of three DGs in continuous working condition variation.

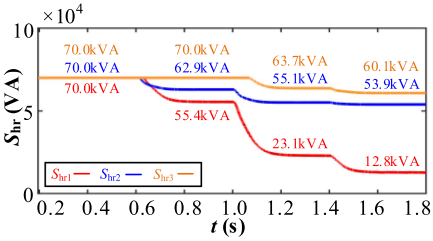

Fig. 14. Harmonic residual power of three DGs in continuous working condition variation.

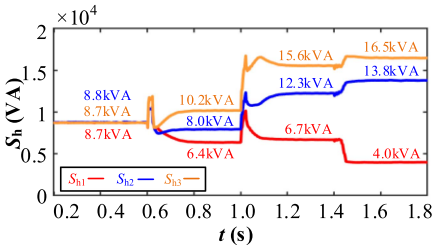

Fig. 15. Harmonic power of three DGs in continuous working condition variation.

different working conditions of fundamental load, the harmonic sharing will be adjusted dynamically based on HRC. With the increase of fundamental load, the fundamental apparent power of three DGs increases, and their HRC decreases, as shown in Figs. 13 and 14.

During 0.2– 0.6 s, S_{hr1}, S_{hr2}, and S_{hr3} are sufficient and the same, which indicates they are in Section I of the droop curve. This corresponds to the condition of light fundamental load. In this case, all the virtual impedance value is set at Z_{omin}, and the harmonic power is equally shared among three DGs, as shown in Fig. 15. Using (8) and (19), the harmonic power sharing error is calculated as

$$\begin{cases} S_{h,1,2} = |\alpha_1 S_{h1} - \alpha_2 S_{h2}| = 0 \\ S_{h,2,3} = |\alpha_3 S_{h3} - \alpha_2 S_{h2}| = 0 \end{cases}. \tag{42}$$

It shows that when the HRC of different DG is the same, equal harmonic sharing can be also realized. This performance is the same as the most of existing research realizing harmonic power sharing according to the rated capacity of DG units. It proves that the proposed novel method also covers the function of traditional methods.

During 0.6–1 s, the S_{hr1} and S_{hr2} are in a normal range, corresponding to Section II, while S_{hr3} is still in Section I of Fig. 8. According to the analysis in Section III-B, this demonstrates the condition of normal fundamental load. In this case, both DG_1 and DG_2 work normally and absorb the harmonic power according to their HRC. The DG_3, which shows adequate HRC will absorb more harmonic power. R_{h1} is equal to 0.160 Ω while R_{h2} is 0.129 Ω, referring to the constant droop coefficient m in (18). R_{h3} is at Z_{omin}, equal to 0.1 Ω.

During 1–1.4 s, all DGs are in Section II of Fig. 8, also corresponding to the condition of normal fundamental load. The harmonic power is shared among three DGs following their HRC.

During 1.4–1.8 s, DG_1 is faced with the risk of overload and S_{hr1} is in Section III, while DG_2 and DG_3 are still in normal condition. S_{hr2} and S_{hr3} are in Section II of Fig. 8. In this case, the virtual impedance of S_{hr1} will rise rapidly according to the accommodation coefficient n_{ac}, as shown in Table III. R_{h1} reaches 0.571 Ω while R_{h2} and R_{h3} are only 0.166 Ω and 0.138 Ω. DG_2 and DG_3 consume much more harmonic power to ensure the safe operation of the microgrid and protect DG_1 from overload.

The sharing error ratio is calculated as (43). In the condition of light fundamental load, the sharing error ratio is almost 0%, indicating a highly accurate equal sharing performance. In the condition of normal and heavy fundamental load, it is less than 5% and is also acceptable

$$\Delta_{S_h - S_{hr}} = \frac{S_{h,i,j}}{S_{hj}} = \frac{|\alpha_i S_{hi} - \alpha_j S_{hj}|}{S_{hj}} \, (1 \le i < j \le 3) \, . \tag{43}$$

2) Virtual Impedance Method Verification: The virtual impedance method verification is composed of fundamental and harmonic parts. The fundamental apparent power of three DGs is shown in Fig. 13, and the ratio of them remains constant in all working conditions. This indicates that R-APF is effective only at selective harmonic and does not affect fundamental power sharing. Therefore, regardless of whether the line impedance is inductive or resistive, R-APF can well adjust harmonic power sharing without affecting fundamental control performance.

The harmonic sharing accuracy of R-APF can be reflected by the sharing error ratio, which is expressed as (44). According to the data in Fig. 15 and Table III, sharing error is around 0% in the condition of light fundamental load, and around 0.5% in the conditions of normal fundamental load and heavy fundamental load, indicating highly accurate harmonic power sharing using R-APF. Thus, the effectiveness of the virtual impedance method is well verified

$$\Delta_{hi-j} = \frac{R_{hi}/R_{hj} - S_{hj}/S_{hi}}{R_{hi}/R_{hj}} \, (1 \le i < j \le 3) \, . \tag{44}$$

3) Dynamic Tradeoff Verification: The existing harmonic sharing strategies have shown an inherent tradeoff between harmonic sharing and power quality. Under the proposed nonlinear harmonic sharing method, the tradeoff is adjusted dynamically. In the condition of light fundamental load, the priority of the control strategy is to improve the power quality of PCC voltage, because the HRC is enough. As shown in Fig. 16, the THD of

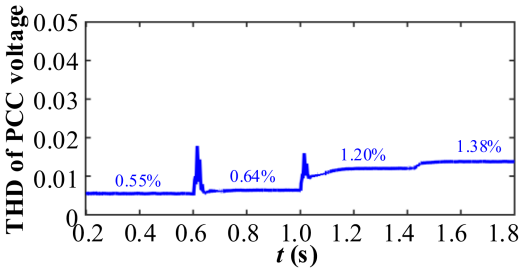

Fig. 16. THD of PCC voltage in continuous working condition variation.

PCC voltage is only 0.55% in light-fundamental-load condition and a good power quality is ensured.

In the condition of normal fundamental load, the harmonic power sharing and power quality of PCC voltage must be considered simultaneously. Thus, the THD is in a normal range and harmonic power sharing according to S_{hr} is also realized. In the heavy fundamental load condition, DG_1 is faced with the risk of being overloaded and the priority of the control strategy is ensuring the safe operation of the microgrid. In this case, the power quality can be sacrificed to some extent. As shown in Fig. 16, PCC power quality further deteriorates and THD reaches 1.38%.

The dynamic adjustment of PCC voltage THD verifies the dynamic tradeoff of the proposed method.

B. Experimental Results

The detailed experimental results in different working conditions of fundamental load are provided further to verify the feasibility and effectiveness of the proposed method. As illustrated in Fig. 17, the microgrid platform includes two DGs and its parameters are listed in Table IV.

Experimental results shown in Figs. 18 to 22 consist of three parts, where (a) is the actual waveform on the oscilloscope, (b) is the DG-current FFT analysis result on the energy analyzer, and (c) is the harmonic power calculated in MATLAB according to the actual data exported from the oscilloscope, respectively. Fig. 23 is the FFT analysis result of PCC voltage, which helps evaluate power quality by THD.

By adding fundamental loads step by step, three working conditions are simulated to verify the proposed method. In addition, to better verify the effectiveness of protecting DG in the heavy fundamental load condition, the harmonic power sharing without and with accommodation coefficient $n_{\rm ac}$ are compared in Figs. 21 and 22. The condition variation and relevant reference value of $R_{\rm h}$ are shown in Table V.

1) Working Condition Without Virtual Impedance: As shown in Fig. 18, before introducing virtual impedance, harmonic power is shared according to the line impedance. In this case, DG_1 with a larger rated capacity absorbs less harmonic power, while DG_2 with a smaller rated capacity should bear more harmonic power. It is unreasonable and DG_2 faces the risk of overload due to the uncontrolled harmonic power. This verifies the motivation of the proposed nonlinear harmonic sharing strategy.

TABLE IV
EXPERIMENTAL PARAMETERS

Symbol	Description	Value
Vdc	Dc voltage	150 V
Vac	the Amplitude of ac output voltage	60 V
$Z_{\rm line1}$	Line impedance of DG_1	1.2 mH
$Z_{\rm line2}$	Line impedance of DG_2	0.6 mH
$R_{\rm load}$	Load resistance	5 Ω
$I_{\rm h5}$	Amplitude of 5th-order harmonic current	8 A
$I_{\rm h7}$	Amplitude of 7th-order harmonic current	3 A
$S_{\rm rate1}$	Rated capacity of DG_1	2400 VA
$S_{\rm rate2}$	Rated capacity of DG_2	2200 VA
$S_{\rm hrs12}$	the Harmonic residual capacity threshold value of section i and section ii	1900 VA
$S_{\rm hrs23}$	the Harmonic residual capacity threshold value of section ii and section iii	900 VA
$Z_{\rm omax}$	the Maximum virtual impedance value of the droop curve in section ii	0.45 Ω
$Z_{\rm omin}$	the Minimum virtual impedance value of the droop curve in section ii	0.15 Ω
m	Constant droop coefficient in section ii	3e-4
$n_{\rm ac}$	Accommodation coefficient	1.25
$k_{\rm p1}$	P-ω droop coefficient of DG_1	5e-5
$k_{\rm p2}$	P-ω droop coefficient of DG_2	5e-5
$k_{\rm q1}$	Q-E droop coefficient of DG_1	1e-3
$k_{\rm q2}$	Q-E droop coefficient of DG_2	1e-3
ω_0	Nominal fundamental frequency	100π rad/s
E_0	Nominal fundamental phase voltage magnitude	60 V
f_s	Switching frequency	20 kHz

TABLE V
WORKING CONDITION VARIATION IN EXPERIMENT

Value of $S_{\rm f}$ and $S_{\rm hr}$	Working Condition	Calculated value of $R_{\rm h}$
$S_{\rm f1}$=1.06 kVA, $S_{\rm f2}$=1.06 kVA $S_{\rm hr1}$=2.15 kVA, $S_{\rm hr2}$=1.93 kVA	Light fundamental load	$R_{\rm h1}$=0.15 Ω $R_{\rm h2}$=0.15 Ω
$S_{\rm f1}$=1.56 kVA, $S_{\rm f2}$=1.56 kVA $S_{\rm hr1}$=1.82 kVA, $S_{\rm hr2}$=1.55 kVA	Normal fundamental load	$R_{\rm h1}$=0.174 Ω $R_{\rm h2}$=0.255 Ω
$S_{\rm f1}$=2.04 kVA, $S_{\rm f2}$=2.04 kVA $S_{\rm hr1}$=1.26 kVA, $S_{\rm hr2}$=0.82 kVA	Heavy fundamental load without $n_{\rm ac}$	$R_{\rm h1}$=0.342 Ω $R_{\rm h2}$=0.475Ω
$S_{\rm f1}$=2.04 kVA, $S_{\rm f2}$=2.04 kVA $S_{\rm hr1}$=1.26 kVA, $S_{\rm hr2}$=0.82 kVA	Heavy fundamental load With $n_{\rm ac}$	$R_{\rm h1}$=0.342 Ω $R_{\rm h2}$=1.4 Ω

2) Working Condition of Light Fundamental Load: In this condition, S_{hr1} and S_{hr2} are sufficient and both virtual impedance is set at $Z_{\rm omin}$, which is 0.15 Ω in the experiment. The harmonic power is almost equally shared between DG_1 and DG_2, as shown in Fig. 19. PCC voltage quality is considered primarily and Fig. 23(a) shows that the THD is 4.1%, satisfying the IEEE standard. By substituting the actual parameter into (44), the harmonic sharing error ratio is calculated as

$$\Delta_{h1-2} = \frac{R_{h2}/R_{h1} - S_{h1}/S_{h2}}{R_{h2}/R_{h1}} = 2.7\%. \tag{45}$$

Equation (43) and Fig. 19 have verified the proposed method works well in the condition of light fundamental load.

3) Working Condition of Normal Fundamental Load: With the increase of fundamental load, the microgrid reaches the normal fundamental load condition. Harmonic power sharing is realized according to the HRC of DGs, which means that DG with a larger HRC absorbs more harmonic power. Both $S_{\rm hr1}$ and $S_{\rm hr2}$ are in Section II of Fig. 8 and the calculated

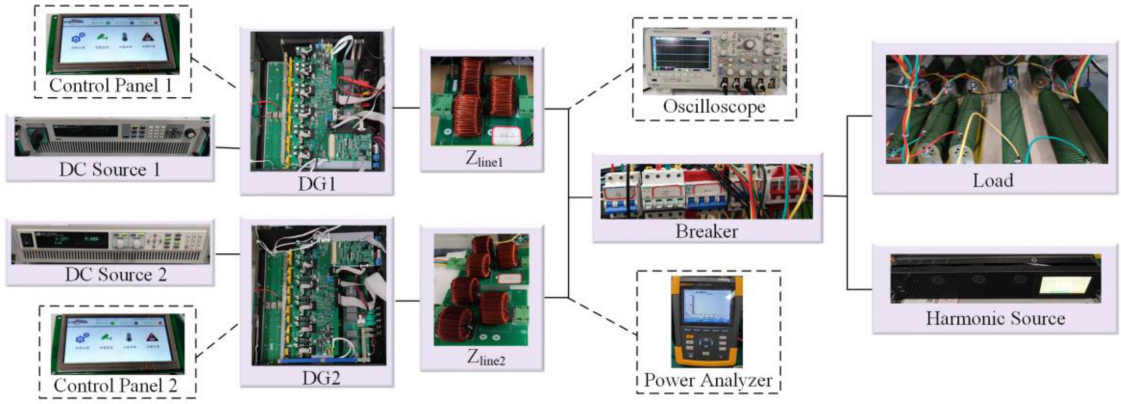

Fig. 17. Microgrid platform in experiment.

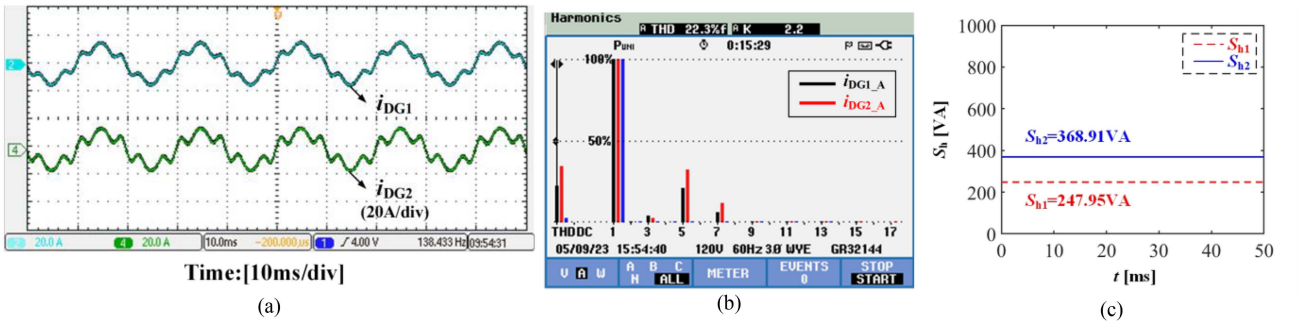

Fig. 18. Working condition without virtual impedance. (a) Harmonic current of DG1 and DG2 in phase A. (b) Harmonic current sharing in energy analyzer. (c) Harmonic power calculated in MATLAB.

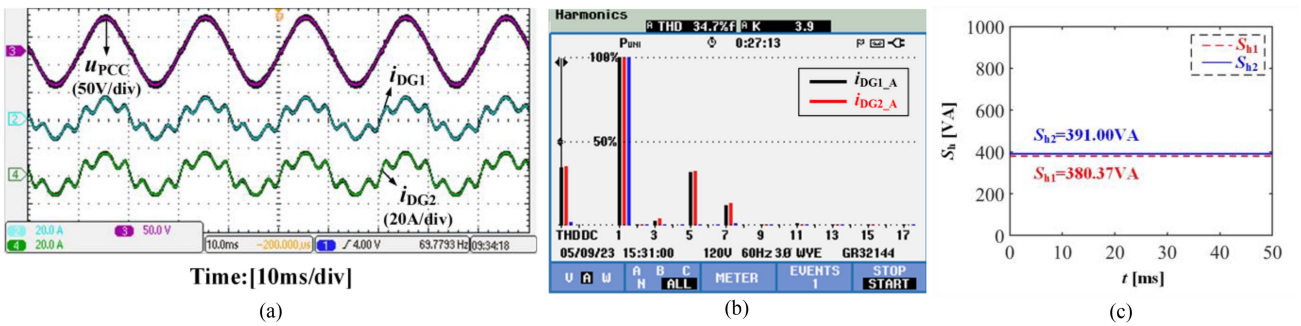

Fig. 19. Working condition of light-fundamental-load. (a) PCC voltage and harmonic current of DG1 and DG2 in phase A. (b) Harmonic current sharing in energy analyzer. (c) Harmonic power calculated in MATLAB.

virtual impedance is 0.174 Ω and 0.255 Ω, respectively. Δ_h is 2.69% in this case, indicating the good performance of the virtual impedance method. The THD of PCC voltage is 4.4%, as shown in Fig. 23(b).

The experimental results in Fig. 20 verify that the proposed nonlinear harmonic sharing strategy works well in the normal-fundamental-load condition and shares the harmonic power by S_{hr}, which is more reasonable and practical than the traditional harmonic power sharing method. It should be noted that when S_{hr1} is equal to S_{hr2}, the harmonic power can be also shared equally.

4) Working Condition of Heavy Fundamental Load: In the condition of heavy fundamental load, DG_2 is faced with the risk of overload, and its virtual impedance should rise rapidly to protect itself from overload. To better verify the effectiveness of the design of variable droop coefficient, the experiment results with and without accommodation coefficient n_{ac} are provided.

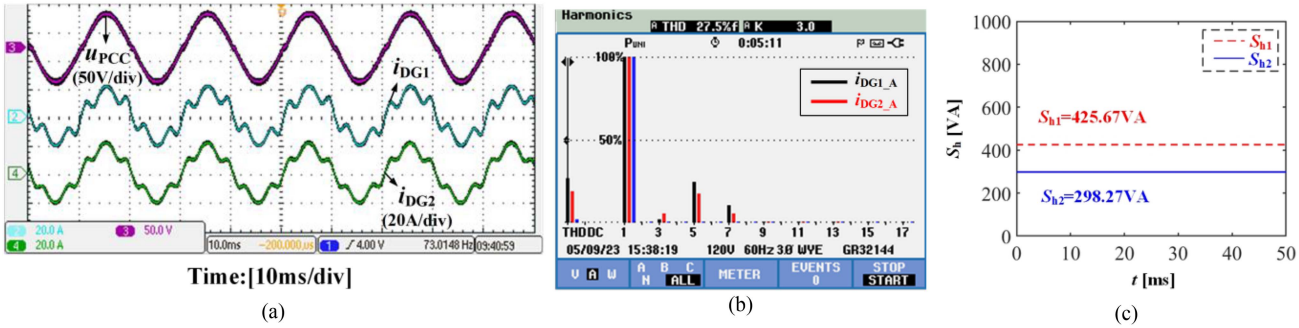

(a) (b) (c)

Fig. 20. Working condition of normal-fundamental-load. (a) PCC voltage and harmonic current of DG1 and DG2 in phase A. (b) Harmonic current sharing in energy analyzer. (c) Harmonic power calculated in MATLAB.

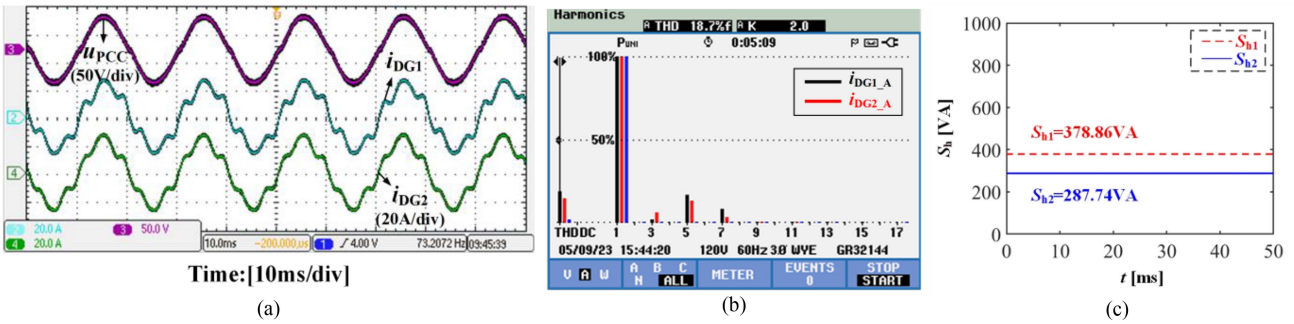

(a) (b) (c)

Fig. 21. Working condition of heavy-fundamental-load before using accommodation coefficient n_{ac}. (a) PCC voltage and harmonic current of DG1 and DG2 in phase A. (b) Harmonic current sharing in energy analyzer. (c) Harmonic power calculated in MATLAB.

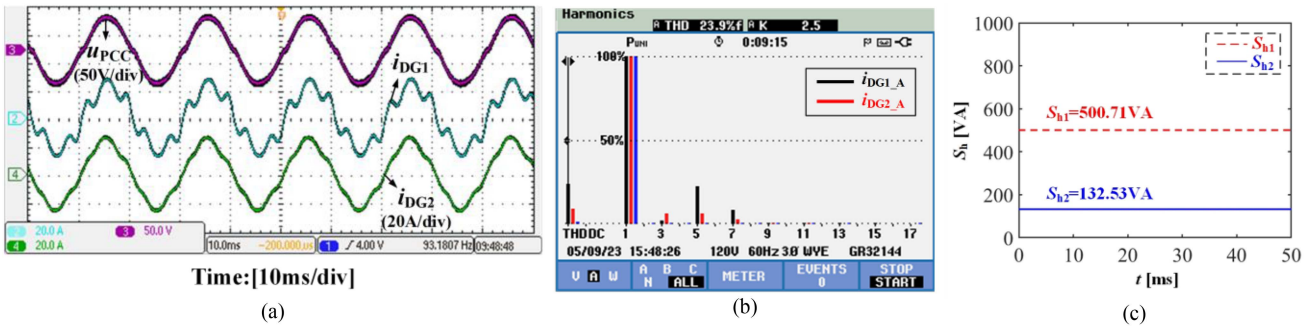

(a) (b) (c)

Fig. 22. Working condition of heavy-fundamental-load after using accommodation coefficient n_{ac}. (a) PCC voltage and harmonic current of DG1 and DG2 in phase A. (b) Harmonic current sharing in energy analyzer. (c) Harmonic power calculated in MATLAB.

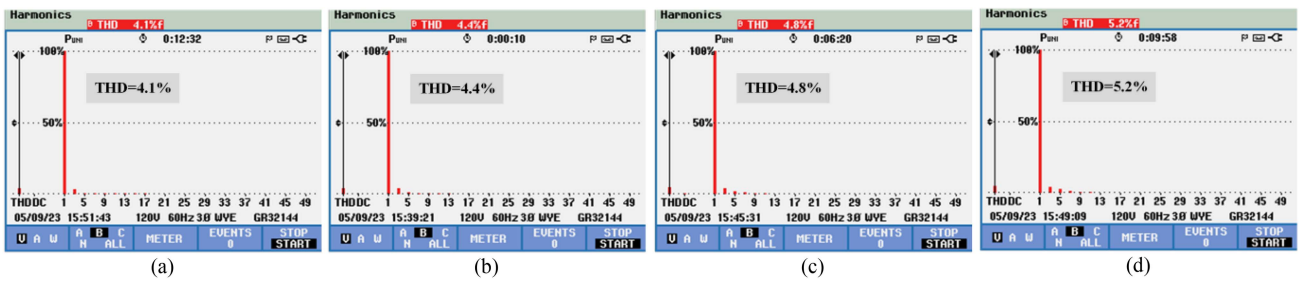

(a) (b) (c) (d)

Fig. 23. THD of PCC voltage. (a) Working condition of light-fundamental-load. (b) Working condition of normal-fundamental-load. (c) Working condition of heavy-fundamental-load before using accommodation coefficient n_{ac}. (d) Working condition of heavy-fundamental-load after using accommodation coefficient n_{ac}.

Fig. 21 shows the performance of the Z_{ref} - S_{hr} droop relationship with a constant coefficient. Though harmonic power flowing into DG_2 is reduced, the risk of overload still exists because the harmonic power is reduced randomly and has nothing to do with the actual residual capacity of DG. On the other hand, Fig. 22 shows the results of a variable droop coefficient. $n_{\rm ac}$ is designed at 2 according to the actual HRC of DG_2. Thus, more than half of harmonic power has been reduced compared with the result in Fig. 21. With this method, the DG_2 can work safely, and optimal utilization of DG capacity is realized. Since the harmonic power consumed by DG_2 is too small compared with the rated value, $\Delta_{\rm h}$ increases to around 6% in this case. However, it is still acceptable. THD of PCC voltage is 5.2%, as shown in Fig. 23(d), which indicates the priority overload protection and the tradeoff in voltage quality.

Figs. 21 and 22 have verified that the proposed nonlinear harmonic power sharing strategy can effectively protect DG from overload in the heavy-fundamental-load condition. It is also proved that the proposed method with a variable droop coefficient is more suitable and reliable than the traditional method with a constant droop coefficient.

In conclusion, the performance of experimental results matches well with the simulation results. The effectiveness and feasibility of the proposed scheme are well verified.

VI. Conclusion

Proper harmonic sharing plays a significant role in the safe and reliable operation of an islanded microgrid. VIA methods are widely used to solve this issue. However, an inherent tradeoff between power quality and harmonic sharing usually exists. Besides, most existing methods share harmonic power according to the rated capacity of the DG, unable to deal with some extreme conditions.

Faced with these issues, based on the nonlinear droop curve between the VIA value and HRC of the DG, a decentralized harmonic sharing scheme is proposed in this article. Under the proposed method, the tradeoff can be adjusted dynamically in different working conditions of fundamental load. Normally, the harmonic sharing is achieved according to the HRC of the DG. In some extreme cases, where a DG faces a great risk of overload, the proposed scheme can automatically adjust the harmonic power flowing into it and protect it from overload.

To sum up, the proposed scheme can realize a flexible harmonic sharing and render an optimal utilization of DG capacity. Furthermore, a dynamic tradeoff under different working conditions of fundamental load is ensured, without deploying any communication lines. The proposed scheme has provided a potential and more flexible solution to the harmonic sharing issue in an islanded microgrid.

In future work, the harmonic sharing issue in the multibus microgrid will be studied. Considering the total THD of the multibus system and the appropriate harmonic sharing, an optimization model will be provided. In addition, conditions where several DGs face overload risk will be discussed. Thus, a more practical control strategy will be designed and a deeper theoretical analysis will be given.

Appendix

In (4), expressions of G_{cv}(s) and Z_{ov}(s) are listed as follows:

$$G_{\rm CV}(s) = \frac{u_{Cf}(s)}{v_{ref}(s)}\Big|_{i_o=0} = \frac{G_o(s)Z_{Cf}(s)G_v(s)}{1+G_o(s)+G_o(s)Z_{Cf}(s)G_v(s)}$$

$$Z_{ov}(s) = -\frac{u_{Cf}(s)}{i_o(s)}\Big|_{v_{ref}=0}$$

$$= \frac{Z_{Cf}(s)\left(1+G_o(s)-Z(s)\right)}{1+G_o(s)+G_o(s)Z_{Cf}(s)G_v(s)}$$

$$G_o(s) = G_i(s)G_{\rm PWM}(s)Y(s).$$

References

[1] A. Hirsch, Y. Parag, and J. Guerrero, "Microgrids: A review of technologies, key drivers, and outstanding issues," *Renewable Sustain. Energy Rev.*, vol. 90, pp. 402–411, Jul. 2018.

[2] M. H. Saeed, W. Fangzong, B. A. Kalwar, and S. Iqbal, "A review on microgrids' challenges & perspectives," *IEEE Access*, vol. 9, pp. 166502–166517, 2021.

[3] J. Hu et al., "Economic model predictive control for microgrid optimization: A review," *IEEE Trans. Smart Grid*, vol. 15, no. 1, pp. 472–484, Jan. 2024.

[4] M. Farrokhabadi et al., "Microgrid stability definitions, analysis, and examples," *IEEE Trans. Power Syst.*, vol. 35, no. 1, pp. 13–29, Jan. 2020.

[5] Y. Qi, H. Deng, X. Liu, and Y. Tang, "Synthetic inertia control of grid-connected inverter considering the synchronization dynamics," *IEEE Trans. Power Electron.*, vol. 37, no. 2, pp. 1411–1421, Feb. 2022.

[6] H. Zheng, Z. Liu, R. An, J. Liu, T. Wu, and Z. Lin, "An islanding detection method using synchronized small-AC-signal injection for grid-forming inverters in microgrids," *IEEE Trans. Power Electron.*, vol. 38, no. 5, pp. 5816–5831, May 2023.

[7] B. Alghamdi and C. A. Cañizares, "Frequency regulation in isolated microgrids through optimal droop gain and voltage control," *IEEE Trans. Smart Grid*, vol. 12, no. 2, pp. 988–998, Mar. 2021.

[8] H. Han, X. Hou, J. Yang, J. Wu, M. Su, and J. M. Guerrero, "Review of power sharing control strategies for islanding operation of AC microgrids," *IEEE Trans. Smart Grid*, vol. 7, no. 1, pp. 200–215, Jan. 2016.

[9] B. Adineh, R. Keypour, P. Davari, and F. Blaabjerg, "Review of harmonic mitigation methods in microgrid: From a hierarchical control perspective," *IEEE J. Emerg. Sel. Topics Power Electron.*, vol. 9, no. 3, pp. 3044–3060, Jun. 2021.

[10] F. Deng, W. Yao, X. Zhang, Y. Tang, and P. Mattavelli, "Review of impedance-reshaping-based power sharing strategies in islanded AC microgrids," *IEEE Trans. Smart Grid*, vol. 14, no. 3, pp. 1692–1707, May 2023.

[11] P. Sreekumar and V. Khadkikar, "Direct control of the inverter impedance to achieve controllable harmonic sharing in the islanded microgrid," *IEEE Trans. Ind. Electron.*, vol. 64, no. 1, pp. 827–837, Jan. 2017.

[12] Z. Wang et al., "Adaptive harmonic impedance reshaping control strategy based on a consensus algorithm for harmonic sharing and power quality improvement in microgrids with complex feeder networks," *IEEE Trans. Smart Grid*, vol. 13, no. 1, pp. 47–57, Jan. 2022.

[13] Z. Wang et al., "Impedance-based adaptively reshaping method for enhancing nonlinear load sharing and voltage quality in islanded microgrids with virtual synchronous generator," *IEEE Trans. Smart Grid*, vol. 13, no. 4, pp. 2568–2578, Jul. 2022.

[14] M. Hamzeh, H. Karimi, and H. Mokhtari, "Harmonic and negative-sequence current control in an islanded multi-bus MV microgrid," *IEEE Trans. Smart Grid*, vol. 5, no. 1, pp. 167–176, Jan. 2014.

[15] Y. Qi, Y. Tang, K. R. R. Potti, and K. Rajashekara, "Robust power sharing control for parallel three-phase inverters against voltage measurement errors," *IEEE Trans. Power Electron.*, vol. 35, no. 12, pp. 13590–13601, Dec. 2020.

[16] J. Chen, L. Wang, L. Diao, H. Du, and Z. Liu, "Distributed auxiliary inverter of urban rail train—Load sharing control strategy under complicated operation condition," *IEEE Trans. Power Electron.*, vol. 31, no. 3, pp. 2518–2529, Mar. 2016.

[17] Y. Wang, X. Zhou, J. Tang, X. Xiao, S. Zhang, and J. Si, "Adaptive harmonic virtual impedance control for improving voltage quality of microgrids," *J. Modern Power Syst. Clean Energy*, early access, doi: 10.35833/MPCE.2023.000447.
[18] A. Micallef, M. Apap, C. Spiteri-Staines, and J. M. Guerrero, "Mitigation of harmonics in grid-connected and islanded microgrids via virtual admittances and impedances," *IEEE Trans. Smart Grid*, vol. 8, no. 2, pp. 651–661, Mar. 2017.
[19] Y. Han, P. Shen, X. Zhao, and J. M. Guerrero, "An enhanced power sharing scheme for voltage unbalance and harmonics compensation in an islanded AC microgrid," *IEEE Trans. Energy Convers.*, vol. 31, no. 3, pp. 1037–1050, Sep. 2016.
[20] F. Göthner, J. Roldán-Pérez, R. E. Torres-Olguin, and O.-M. Midtgård, "Harmonic virtual impedance design for optimal management of power quality in microgrids," *IEEE Trans. Power Electron.*, vol. 36, no. 9, pp. 10114–10126, Sep. 2021.
[21] T. V. Hoang and H.-H. Lee, "Virtual impedance control scheme to compensate for voltage harmonics with accurate harmonic power sharing in islanded microgrids," *IEEE J. Emerg. Sel. Topics Power Electron.*, vol. 9, no. 2, pp. 1682–1695, Apr. 2021.
[22] H. H. Goh et al., "Harmonic virtual impedance control in islanded microgrids for harmonic power sharing and harmonic suppression," *CSEE J. Power Energy Syst.*, early access, doi: 10.17775/CSEEJPES.2022.06150.
[23] J. Lu, M. Zhao, S. Golestan, T. Dragicevic, X. Pan, and J. M. Guerrero, "Distributed event-triggered control for reactive, unbalanced, and harmonic power sharing in islanded AC microgrids," *IEEE Trans. Ind. Electron.*, vol. 69, no. 2, pp. 1548–1560, Feb. 2022.
[24] F. Deng, X. Li, X. Zhang, and P. Mattavelli, "An iterative virtual impedance regulation strategy in islanded microgrids for enhanced balanced, unbalanced and harmonic current sharing," *IEEE Trans. Sustain. Energy*, vol. 13, no. 1, pp. 514–526, Jan. 2022.
[25] J. Xiao, L. Wang, P. Bauer, and Z. Qin, "Virtual impedance control for load sharing and bus voltage quality improvement in low-voltage AC microgrid," *IEEE Trans. Smart Grid*, vol. 15, no. 3, pp. 2447–2458, May 2024.
[26] Y. Zhu, F. Zhuo, F. Wang, B. Liu, R. Gou, and Y. Zhao, "A virtual impedance optimization method for reactive power sharing in networked microgrid," *IEEE Trans. Power Electron.*, vol. 31, no. 4, pp. 2890–2904, Apr. 2016.
[27] A. H. Yazdavar, M. A. Azzouz, and E. F. El-Saadany, "A novel decentralized control scheme for enhanced nonlinear load sharing and power quality in islanded microgrids," *IEEE Trans. Smart Grid*, vol. 10, no. 1, pp. 29–39, Jan. 2019.
[28] B. Liu, Z. Liu, J. Liu, R. An, H. Zheng, and Y. Shi, "An adaptive virtual impedance control scheme based on small-AC-signal injection for unbalanced and harmonic power sharing in islanded microgrids," *IEEE Trans. Power Electron.*, vol. 34, no. 12, pp. 12333–12355, Dec. 2019.
[29] J. Roldán-Pérez, M. Prodanovic, A. Rodríguez-Cabero, J. M. Guerrero, and A. García-Cerrada, "Finite-gain repetitive controller for harmonic sharing improvement in a VSM microgrid," *IEEE Trans. Smart Grid*, vol. 10, no. 6, pp. 6898–6911, Nov. 2019.
[30] R. Razi, H. Iman-Eini, M. Hamzeh, and S. Bacha, "A novel extended impedance-power droop for accurate active and reactive power sharing in a multi-bus microgrid with complex impedances," *IEEE Trans. Smart Grid*, vol. 11, no. 5, pp. 3795–3804, Sep. 2020.
[31] M. Zhang, B. Song, and J. Wang, "Circulating current control strategy based on equivalent feeder for parallel inverters in islanded microgrid," *IEEE Trans. Power Syst.*, vol. 34, no. 1, pp. 595–605, Jan. 2019.
[32] S. Y. Mousazadeh Mousavi, A. Jalilian, M. Savaghebi, and J. M. Guerrero, "Autonomous control of current- and voltage-controlled DG interface inverters for reactive power sharing and harmonics compensation in islanded microgrids," *IEEE Trans. Power Electron.*, vol. 33, no. 11, pp. 9375–9386, Nov. 2018.
[33] Z. Zeng, H. Yi, F. Zhuo, and Z. Wang, "A new control scheme based on R-APF for harmonic power sharing in islanded microgrids," in *Proc. IEEE Energy Convers. Congr. Expo.*, 2017, pp. 2991–2995.
[34] *IEEE Standard Definitions for the Measurement of Electric Power Quantities Under Sinusoidal, Nonsinusoidal, Balanced, or Unbalanced Conditions*, IEEE Std 1459-2010, 2010.
[35] U. Manandhar et al., "Energy management and control for grid connected hybrid energy storage system under different operating modes," *IEEE Trans. Smart Grid*, vol. 10, no. 2, pp. 1626–1636, Mar. 2019.

Xiao Zhang (Student Member, IEEE) received the B.S. degree in electrical engineering and automation from Central South University, Changsha, China, in 2019. He is currently working toward the Ph.D. degree in electrical engineering with Xi'an Jiaotong University, Xi'an, China.

His research interests include power quality control, energy storage, and control strategy of microgrid.

Hao Yi (Member, IEEE) received the Ph.D. degree in electrical engineering from Xi'an Jiaotong University (XJTU), Xi'an, China, in 2013.

He visited the Department of Energy Technology, Aalborg University, Aalborg, Denmark, from 2016 to 2017. He is currently an Associate Professor with XJTU. He hosted one prize and published more than 70 articles on the topics of his research interests, which include power electronics technologies used in power quality control and grid-connected converter modeling/control.

Ya Wen received the B.S. degree in electrical engineering and automation from Sichuan University, Chengdu, China, in 2022. She is currently working toward the M.S. degree in electrical engineering with Xi'an Jiaotong University, Xi'an, China.

Her research interests include power quality control and microgrid.

Zhenxiong Wang (Member, IEEE) received the B.S. and Ph.D. degrees in electrical engineering from Xi'an Jiaotong University, Xi'an, China, in 2014 and 2021, respectively.

He is currently an Assistant Professor with Xi'an Jiaotong University. His research interests include grid-forming control strategy and microgrid.

Qiru Li received the B.S. degree in electrical engineering and automation from Xi'an Jiaotong University, Xi'an, China, in 2022. He is currently working toward the master's degree in electrical engineering with Xi'an Jiaotong University, Xi'an, China.

His research interest includes power quality control.

Fangrui Kang received the B.S. degree in automation from Xidian University, Xi'an, China, in 2022. She is currently working toward the M.S. degree in electrical engineering with Xi'an Jiaotong University, Xi'an, China.

Her research interests include power quality control and energy storage.

Fang Zhuo (Member, IEEE) was born in Shanghai, China, in 1962. He received the B.S. degree in automatic control and the M.S. and Ph.D. degrees in automation and electrical engineering, from Xi'an Jiaotong University (XJTU), Xi'an, China, in 1984, 1989, and 2001, respectively.

He was an Associate Professor in 1996 with XJTU, where he became a Full Professor in power electronics and drives in 2004. Then, he was a Supervisor of Ph.D. students. He is the key finisher of the four projects sponsored by the National Natural Science Foundation of China, more than 40 projects cooperated with companies from the industry and holds four patents. His research interests include power electronics, power quality, active power filter, reactive power compensation, and inverters for distributed power generation.

Dr. Zhuo was the recipient of four provincial- and ministerial-level science and technology advancement awards. He is a member of the China Electro Technical Society, Automation Society, and Power Supply Society. He is also the Power Quality Professional Chairman of the Power Supply Society in China.